analytical chemistry

Article

Cite This: Anal. Chem. 2018, 90, 12456−12463

pubs.acs.org/ac

Electrochemical and Surface-Plasmon Correlation of a Serum-Autoantibody Immunoassay with Binding Insights: Graphenyl Surface versus Mercapto-Monolayer Surface

Gayan Premaratne,[†,⊥] Jinesh Niroula,[†,⊥] Manoj K. Patel,[†,¶] Wei Zhong,[‡] Steven L. Suib,[‡] A. Kaan Kalkan,[§] and Sadagopan Krishnan*[,†]

[†]Department of Chemistry, Oklahoma State University, Stillwater, Oklahoma 74078, United States

[‡]Department of Chemistry, University of Connecticut, Storrs, Connecticut 06269, United States

[§]Department of Mechanical and Aerospace Engineering, Oklahoma State University, Stillwater, Oklahoma 74078, United States

Supporting Information

ABSTRACT: We present here the correlation of picomolar affinities between surface-plasmon and electrochemical immunoassays for the binding of serum glutamic acid decarboxylase 65 autoantibody (GADA), a biomarker of type 1 diabetes (T1D), to its antigen GAD-65. Carboxylated (∼5.0%)-graphene-modified immunoassembly on a gold surface-plasmon chip or on an electrochemical array provided significantly larger binding affinity, higher sensitivity, and lower detection limits than a self-assembled monolayer surface of mercaptopropionic acid (MPA). Estimation of the relative surface −COOH groups by covalent tagging of an electroactive aminoferrocene showed that the graphenyl surface displayed a greater number of −COOH groups (9-fold) than the MPA surface. X-ray-photoelectron-spectroscopy analysis showed more C−O and C═O functionalities on the graphene-COOH surface than on the MPA surface. The graphene-COOH coating on gold exhibited ∼5.5-fold enhancement of plasmon signals compared with a similar coating on a plain glass surface. In summary, this article provides a quantitative comparison of carboxylated graphene with a mercapto-monolayer immunoassembly. Additionally, we propose that the binding-constant value can be useful as a quality-control checkpoint for reproducible and reliable production of large-scale biosensors for clinical bioassays.

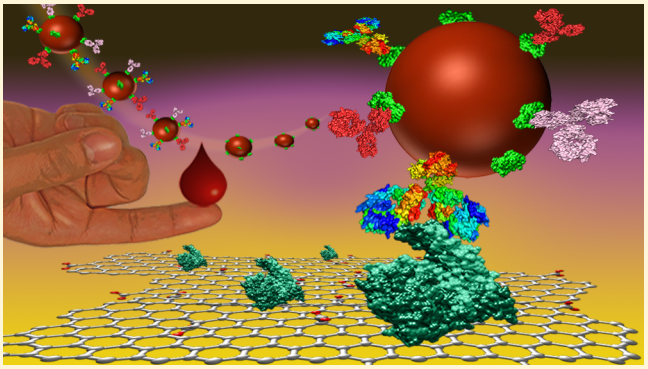

The design of a reliable and reproducible biosensing-assay platform with molecular insights into binding and quantitative nanobiosurface design is significant for successful diagnostic applications. Serum concentration of autoantibodies has been proposed to be associated with the occurrence of type 1 diabetes (T1D).[1,2] T1D is a chronic immune disorder that results from the destruction of β-cell function in the islets of Langerhans, in which deficient insulin levels raise blood glucose levels as a result of impaired glucose metabolism (hyperglycemia).[3] The etiology of T1D is largely unknown, but a combination of genetic predisposition, environmental factors, and a dysregulated immune system is believed to be the cause of the disorder.[4−6] Over recent years, the prevalence of diabetes, in particular T1D has significantly increased from 5 to 10%. This has in turn affected the incidence of associated health complications on a large population of children and adults worldwide.[7,8]

Pociot and Lernmark recently reported that the appearance of certain autoantibodies at an early age can act as a triggering factor for T1D, and glutamic acid decarboxylase 65 autoantibody (GADA) is one of them.[9] In the early 1990s, GADA was recognized as interacting with a 65 kDa autoantigen known as glutamic acid decarboxylase 65 (GAD-65). Later, Urban and co-workers reported the association of GAD-65−GADA immune complexes with stiff syndrome and T1D.[10] GADA has been recognized as a highly valuable biomarker for the prediction of T1D and thus is significant for the development of simple and accurate methods for early diagnosis of T1D.

In the past, several research groups demonstrated methods for the clinical diagnosis of T1D, including radioimmunoassays (RIAs),[11] enzyme-linked immunosorbent assays (ELISAs),[12] chemiluminescent immunoarrays (CLIAs),[13] and electrochemiluminescence assays.[14] Here, we use an inexpensive ferricyanide reagent to accomplish the electrochemical detection of GADA, determine the binding constants and analytical-assay parameters, and provide quantitative insights into carboxylated-graphene and mercapto-monolayer surface modifications (Scheme 1).

Received: April 7, 2018
Accepted: September 14, 2018
Published: September 14, 2018

DOI: 10.1021/acs.analchem.8b01565
Anal. Chem. 2018, 90, 12456−12463

Scheme 1. Graphenyl- and Mercapto-Monolayer-Based Immunosensor Designs for Comparative Analysis[a]

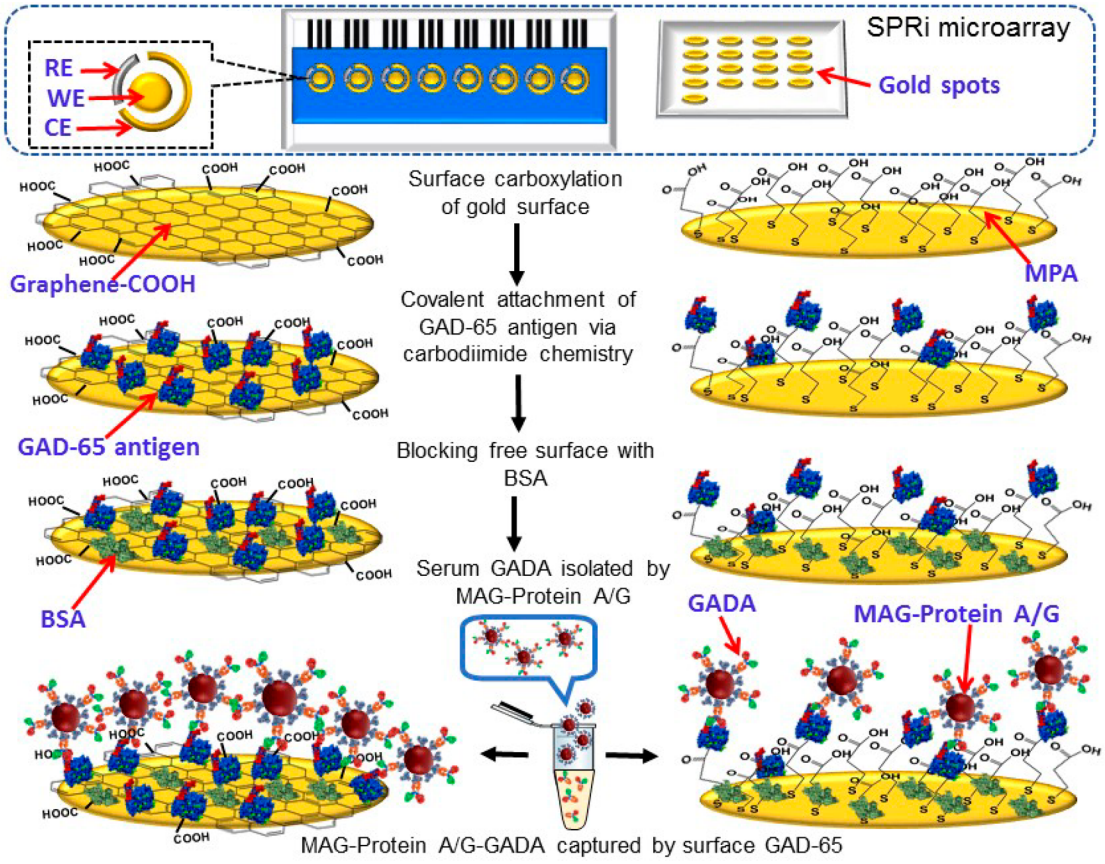

[a]WE, gold working electrode; CE, gold counter electrode; RE, pseudo-silver reference electrode.

As a novel class of a two-dimensional nanocarbon material, graphene has recently attracted researchers in biomedical sciences for the development of electrochemical and optical devices.[15−17] Its high surface-area-to-volume ratio, electrical conductivity, and aqueous dispersibility make it suitable for screen-printed electrode surfaces, and the thin structure and apparent biocompatibility of carboxylated graphene makes it a unique carbon nanomaterial for biorecognition events and biosensing applications.[18−20] Although, glucose and insulin biosensors are useful for diabetes management, nonglucose biomarkers are critical for enabling early diabetes detection in children and adults.[21−23]

To increase detection sensitivity, modification of sensor surfaces with various nanomaterials and selective isolation of analytes from complex sample matrices (e.g., blood, saliva, and urine) by nanomaterials for amplified detection were developed.[24−29] In particular, magnetic (MAG) beads are unique for the ease of magnetic isolation and separation and highly sensitive detection of proteins, nucleic acids, and cells as a result of their high surface areas and intrinsic magnetic properties.[30−34]

Appropriate design of the surfaces of MAG beads with specific capture molecules can be used to separate biomolecules selectively from complex clinical matrices to facilitate ultralow detection with reduced nonspecific signals.[30,31,35−37] In the present study, we demonstrate that by combining electrochemical immunosensing with surface-plasmon-resonance (SPR) spectroscopy, we can validate the electrochemical platform and use the binding constant as a quality-control checkpoint for the large-scale production of relatively less expensive electrochemical sensors.

Furthermore, in this work, a carboxylated-graphenyl surface is quantitatively compared with the conventional mercapto-monolayer surface to obtain insights into analytical-assay performance. The knowledge gained from the combined sensing and binding assessment is useful for developing reliable and higher-throughput clinical immunosensors for biomarker-based diagnostic assays.

EXPERIMENTAL SECTION

Reagents and Materials. Eight-channel screen-printed gold electrodes (8×SPE) were purchased from DropSens Inc. (product no. 8×220BT; Llanera, Spain). SPR imaging (SPRi) gold array chips (Spot Ready 16, 1 mm diameter gold spots) were purchased from GWC Technologies (Madison, WI). Carboxylated graphene (graphene-COOH) was purchased from ACS materials (Medford, MA). Glutamic acid decarboxylase 65 antigen (GAD-65) was bought from Creative Diagnostics (Shirley, NY). Monoclonal glutamic acid decarboxylase 65 autoantibody (GADA), bovine serum albumin (BSA, ≥ 98%), aminoferrocene, 3-mercaptopropionic acid (MPA, ≥ 99%), 1-ethyl-3-[3-(dimethylamino) propyl] carbodiimide (EDC), and *N*-hydroxysuccinimide (NHS) were purchased from Sigma (St. Louis, MO). Normal human serum was purchased from Atlanta Biologicals (Flowery Branch, GA).

Human serum samples were diluted 10 times in phosphate-buffered saline. Protein A/G coated magnetic beads (MAG−

DOI: 10.1021/acs.analchem.8b01565
Anal. Chem. 2018, 90, 12456−12463

protein A/G, 2 μm, 10 mg mL^{-1}) were purchased from Biotool (Houston, TX). The beads contained 9.3 × 10^{13} protein A/G molecules cm^{-2} (Biotool). All other chemicals used were analytical grade. A NanoOrange Protein Quantitation Kit was purchased from Thermo Fisher Scientific (Waltham, MA). The commercial GADA ELISA kit was purchased from MyBioSource, Inc. (San Diego, CA). The reagents were prepared using ultrapure water (Invitrogen Corporation, Grand Island, NY). All measurements were conducted at room temperature (23 °C).

Methods. Detailed experimental procedures are presented in the Supporting Information.

Immobilization of GAD-65 Antigen on Carboxylated Gold Surfaces. Briefly, standard carbodiimide chemistry was followed to covalently link the surface lysine groups of GAD-65 (PDB: 2OKK, ~29 surface lysine residues) to the carboxyl groups available on the electrode surface from graphene-COOH or MPA.[38−40] Isolation of GADA from 10% serum was accomplished by using protein A/G functionalized 2 μm MAG beads.

Magnetic Bead−Protein A/G Capturing of Autoantibody from 10% Human Serum (MAG−protein A/G−GADA). MAG beads functionalized with surface protein A/G molecules offer binding sites oriented correctly for capturing antibodies from serum. The capturing procedure followed the instructions provided by the manufacturer with slight modifications. In brief, 25 μL of MAG−protein A/G beads was washed twice with 150 μL of phosphate-buffered saline (PBS, pH 7.4; 10 mM phosphate; 0.14 M NaCl; 2.7 mM KCl) and separated out using a small piece of magnet after each wash. Then, the beads were washed twice in 150 μL of binding buffer (50 mM tris, 150 mM NaCl, 0.1% Tween 20, pH 7.5). Different concentrations of GADA spiked in 10% normal human serum in the binding buffer (250 μL) were added to separate aliquots of MAG−protein A/G beads and rotated in a tube rotor (Fisher Scientific, Waltham, MA) for 1 h at room temperature. Upon completion of the incubation, the contents were suspended by pipetting up and down 10 times, and the supernatant was removed immediately from the magnetically separated beads. The beads were washed two times with 300 μL of the binding buffer. Finally, the beads were suspended to a final volume of 200 μL in the binding buffer. The MAG−protein A/G captured serum-GADA samples were stored at 4 °C and used for up to 5 days.

QCM Estimation of Immobilized GAD-65. To obtain a quantitative estimation of the amount of surface-immobilized GAD-65 on the graphene-COOH or MPA surface, we used a quartz-crystal-microbalance (QCM) technique. The oscillation-frequency decrease was monitored in real-time in the QCM instrument in proportion to the mass added from the covalent immobilization of GAD-65 (Gamry Instruments Inc., Warminster, PA).

Quantitation of Serum GADA and Assessment of Binding Insights. Electrochemical-impedance-spectroscopy (EIS) measurements were performed to characterize the modification of the sensor surface as well as to measure the GADA-concentration-dependent increase in charge-transfer resistance (R_{ct}) for the ferricyanide/ferrocyanide redox probe added in solution. For the EIS, an Interface 1000 potentiostat/galvanostat/ZRA from Gamry Instruments was used (Warminster, PA).

Surface-plasmon measurements of the GADA−GAD-65 interaction were made using a GWC SPR imager-II (Horizon SPR imager model, GWC Technologies, Madison, WI). A light source with an operating wavelength of 800 nm was used. Real-time reflectivity changes were measured using a charge-coupled device followed by imaging of these changes in terms of the pixel intensity. The SPR curves were fit for kinetic analysis using TraceDrawer Software (Ridgeview Instruments AB, Vänge, Sweden).

Differential-pulse-voltammetric (DPV) and cyclic-voltammetric measurements were made using a CHI 1040C eight-channel electrochemical workstation (Austin, TX). The DPV was used as a complementary method to EIS to determine K_D values. Cyclic voltammetry was used for the quantitation of the surface carboxyl groups of graphene-COOH and MPA by aminoferrocene derivatization of the −COOH groups.

ELISA measurements were performed using a Biotek Synergy H1 Plate Reader on the basis of UV−vis-fluorescence quantitation (BioTek Instruments, Inc., Winooski, VT).

RESULTS AND DISCUSSION

Immunosensor Optimization and Characterization. Faradaic EIS using a constant binding concentration of serum GADA (4 ng mL^{-1}) captured on MAG−protein A/G beads was used to determine the optimum concentration of GAD-65. Figure S1 shows the graphene-COOH-modified GAD-65 immobilized immunosensor response for the binding of GADA (4 ng mL^{-1}) captured onto the MAG−protein A/G beads. No appreciable change in the R_{ct} was observed beyond 6.5 μg mL^{-1} GAD-65. Therefore, we chose this solution concentration of GAD-65 to immobilize on the designed graphene-COOH surface for the immunosensor design.

Hydrodynamic-size and zeta-potential measurements displayed an increase in the average hydrodynamic size and a negative shift in the zeta potential of the MAG−protein A/G beads after they captured serum GADA (Table S1). Scanning-electron-microscopy (SEM), FTIR-ATR-spectroscopy, and EIS characterizations confirmed the successful design of the graphene-COOH-modified immunosensors (Figures S2−S4, details in the Supporting Information).

Serum-GADA-Concentration-Dependent Increase in Charge-Transfer Resistance. The Faradaic-impedance responses and the respective calibration plots are presented in Figure 1. The R_{ct} of the GAD-65 sensor surface increased with increasing serum GADA concentrations (10% serum in PBS) captured with the MAG−protein A/G beads. This trend suggests that the increase in surface-bound GADA, carried by the MAG−protein A/G beads from the specific complexation with GAD-65-antigen sites, increased the resistance to the ferri/ferrocyanide redox probe in solution over that of the control serum treated with magnetic−protein A/G beads (no spiked GADA).

In order to estimate the detection-sensitivity enhancement by the graphene-COOH modification compared to a conventional self-assembled monolayer surface on gold, we prepared MPA-monolayer-modified 8×SPE arrays. An immunoassembly similar to that of graphene-COOH was constructed for the MPA modification, and the R_{ct} signals were measured.

The results imply that the graphenyl sensor displayed a wider dynamic range of 0.02−2 ng mL^{-1} and increased R_{ct} values by several thousands over those of the MPA-monolayer-modified sensor (0.04−0.75 ng mL^{-1}) for the same GADA concentration. The slope of the response curve in the linear range corresponds to the sensitivity of the sensor. A sensitivity enhancement of about 3-fold was observed for the graphenyl

DOI: 10.1021/acs.analchem.8b01565
Anal. Chem. 2018, 90, 12456−12463

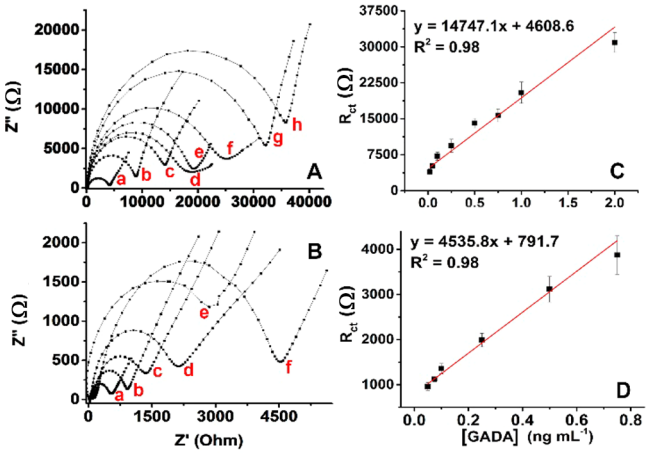

Figure 1. (A,B) Nyquist plots obtained from Faradaic-impedance measurements in an aqueous solution containing 0.1 M KCl and 10 mM $Fe(CN)_6^{3-}/Fe(CN)_6^{4-}$ (each) for various concentrations of surface-bound-serum-GADA immunoassembly on (A) graphene-COOH-modified immunosensors (0.02, 0.05, 0.1, 0.25, 0.5, 0.75, 1.0, and 2.0 ng mL^{-1}, curves a–h, respectively) and (B) MPA-modified immunosensors (0.02, 0.05, 0.1, 0.25, 0.5, and 0.8 ng mL^{-1}, curves a–f, respectively). (C,D) Dynamic ranges of the respective response plots for R_{ct} changes vs the concentration of GADA for N = 5 replicates. Serum (10%) not spiked with any GADA but treated with the MAG–protein A/G beads was used as the control sample, and its R_{ct} value was subtracted from each of the GADA-spiked-serum-sample responses. The experimental conditions were 0.2 V vs pseudo-Ag reference electrode, amplitude of 10 mV, and frequency range of 0.1–100 kHz.

surface over the MPA-modified surface (slopes in Figure 1C,D), which is quite significant for just 5% carboxylated graphene.

The detection limits (3 times the standard deviation of the control response divided by the slope of the calibration graph) were 48 and 124 pg mL^{-1} for the graphenyl- and MPA-modified immunosensors, respectively. It is evident that the large surface area and –COOH functional groups on graphene-COOH are favorable for the high-density immobilization of surface biomolecules for the detection of lower concentrations of analytes, compared with the MPA-monolayer sensor. The clinically relevant serum-GADA-concentration range has been reported to be 0.03–19.9 nM or 1.95 ng mL^{-1} to 1.29 μg mL^{-1}.[41] Saturation behavior on the assay response was observed beyond 2 ng mL^{-1} serum GADA. Although, higher concentrations of GADA will require dilution before measurement in the designed assay platform, several biomarkers with clinically relevant low-nanomolar concentrations can directly benefit from the assay.

Additionally, although protein A/G is not selective for capturing GADA alone but captures all serum antibodies, the designed immunosensor is successful in measuring low GADA concentrations above the nonspecific control serum-treated MAG-bead signals (no spiked GADA).

Estimation of Signal Enhancement and Reduction of Nonspecific Signals by the MAG–Protein A/G Beads over the Direct Use of a Serum-GADA Solution. Figure 2A shows that the R_{ct}-signal enhancement for the binding of 2 ng mL^{-1} serum GADA captured with MAG–protein A/G beads was ~3-times greater than the direct use of GADA-spiked 10% serum solution samples not captured onto the beads. Figure 2B shows that the nonspecific control response is

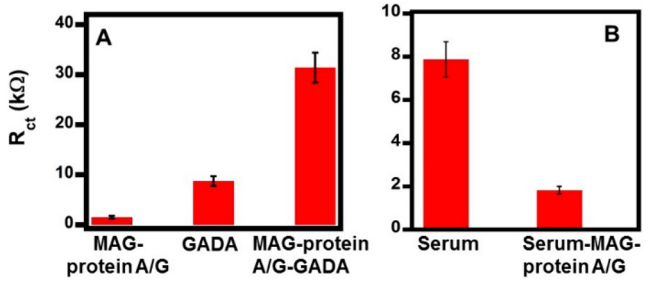

Figure 2. (A) R_{ct} values for the BSA-blocked, graphene-COOH-coated-gold-surface-immobilized GAD-65 upon the binding of MAG–protein A/G beads alone (1.25 mg mL^{-1}), GADA (2 ng mL^{-1}) spiked in 10% serum in PBS (pH 7.4), and serum GADA (2 ng mL^{-1}) captured onto the MAG–protein A/G beads. (B) Reduced nonspecific-serum-matrix signals for MAG–protein A/G incubated with and isolated from 10% serum over those of the free-serum solution after treatment with the surface-immobilized GAD-65 antigen.

greater for the unspiked 10% serum bound to the surface GAD-65 antigen than for the corresponding MAG–protein A/G beads incubated with the serum control.

The results indicate that the MAG–protein A/G bead strategy for isolating GADA from serum reduced the nonspecific background signals from proteins and other components present in the free-serum matrix and thus offered enhanced sensitivity (Figure 2A).[33,42–44] The simplicity of the magnetic capturing and isolation of bound GADA from free serum by the MAG–protein A/G beads is not feasible with other nonmagnetic nanomaterials,[45] which would require centrifugation or other tedious separation procedures.

SPRi Pixel Intensities for Various Serum GADA Concentrations. The low dielectric permittivity and intrinsic graphene plasmonics with the ability to modulate the evanescent wave[46,47] allowed us to construct the same electrochemical immunosensor assembly on an SPR gold-array chip to validate the electrochemical assay and additionally obtain binding-kinetic parameters. Increases in SPRi pixel intensities with increased concentrations of serum GADA for graphene-COOH- and MPA-modified immunosensors are illustrated in Figure 3A,B, respectively. The nonspecific-binding signal for MAG–protein A/G treated serum with no spiked GADA was taken as the control response, similar to the electrochemical assay. The control signal was lower for the graphene-COOH sensor compared with the MPA-modified sensor, indicating that the BSA-blocked graphene-COOH surface is better than the conventional gold–MPA surface at minimizing nonspecific signals. Moreover, the results confirm that the assay specificity relies on the selective GADA–GAD-65 interaction.

Figure 3C shows the linear ranges of the SPRi-response plots for varying concentrations of 10% serum GADA captured onto MAG–protein A/G beads and immunoassembled with the surface GAD-65 on the graphene-COOH- and MPA-modified sensors. The graphene-COOH-modified sensor was almost 2 times more sensitive than the MPA-modified sensor. For the graphene-COOH sensor, the SPRi dynamic range was 0.01–1.25 ng mL^{-1} with a detection limit 3 times lower (6.5 pg mL^{-1}) than that of the MPA sensor, which had a dynamic range of 0.01–1.00 ng mL^{-1} and a detection limit of 18.8 pg mL^{-1}. A similar trend to that of the electrochemical immunosensor is evident. Thus, appropriate design of the

DOI: 10.1021/acs.analchem.8b01565
Anal. Chem. 2018, 90, 12456–12463

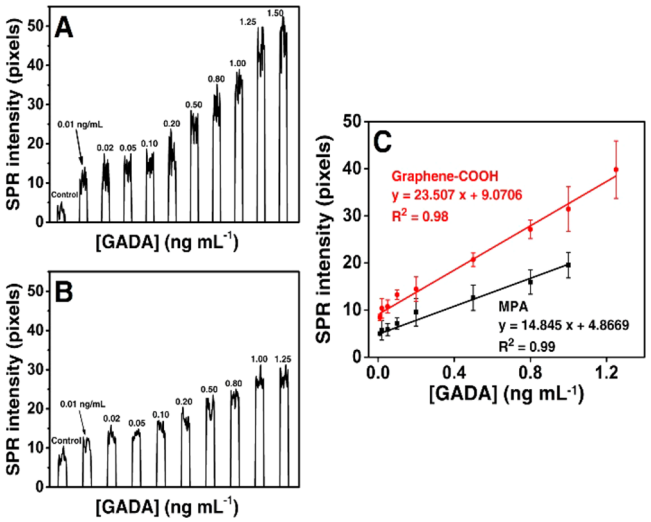

Figure 3. SPRi pixel intensities for different concentrations of serum GADA captured by MAG−protein A/G beads and bound to GAD-65 antigen immobilized on (A) graphene-COOH- and (B) MPA-modified gold array chip. Control responses correspond to signals for the binding of 10% serum treated with MAG−protein A/G beads not spiked with GADA. (C) Control-subtracted SPRi-response plots with concentrations of serum GADA for the GAD-65-immobilized graphene-COOH or MPA surface.

gold SPRi chip for use as an electrode array and interfacing of the SPRi with a potentiostat unit will offer a combined-assay approach.

To illustrate the plasmonic-enhancement property of graphene-COOH on the Au surface of the designed sensor,[48] we performed Raman-spectral analysis of the graphene-COOH coated on the gold surface of an SPRi chip and compared the spectral peak intensity with that of graphene-COOH similarly coated on plain glass instead of gold (Figure S5). The Raman-signal enhancement for the D and G bands on the graphene-COOH-coated gold was higher than on the glass surface. The increase in Raman signals has been proposed to be due to a charge-transfer process from the graphenyl material to the gold-metal surface resulting in the coupling of metal plasmons with graphene plasmons and the associated enhancement of electromagnetic fields.[26,47]

Determination of Kinetic Parameters from the Real-Time Binding of Surface-Immobilized GAD-65 to MAG−Protein A/G Beads Captured Serum GADA. The experimentally obtained SPR sensograms (Figure S6A,B) for different concentrations of GADA were fit into a 1:1 bimolecular kinetic model.[33,49] The equations presented in the Supporting Information were used to calculate the association-rate (k_a), the dissociation-rate (k_d), and the binding-constant (K_D) parameters (Table 1).

Table 1. Kinetic Parameters for the Binding of MAG−Protein A/G Beads−Captured Serum GADA onto Surface-Immobilized GAD-65 Antigen

kinetic parameters	graphene-COOH	MPA
association rate constant, k_a [M^{-1} s^{-1}]	(1.05 ± 0.13) × 10^9	(0.90 ± 0.13) × 10^9
dissociation rate constant, k_d [s^{-1}]	(3.2 ± 0.4) × 10^{-3}	(5.0 ± 0.6) × 10^{-3}
binding constant, K_D [pM]	3.0 ± 0.5	5.6 ± 1.0

The lower K_D value for the graphene-COOH-modified SPRi chip suggests that graphene provides a stronger GADA−GAD-65 binding interaction (i.e., a more sensitive platform from an analytical perspective) through its increased number of surface carboxyl groups and its plasmon-enhancing feature when compared with the MPA-modified chip. Moreover, the K_D values of both MPA- and graphene-COOH-modified chips are smaller (better affinity) in comparison with the previously reported SPR assay value (K_D = 1.37 nM) in PBS-buffer medium on the surface of a mixed self-assembled monolayer.[50] This is likely due to the signal enhancements from the MAG−protein A/G bead strategy offering a highly enhanced signal output compared with that of free GADA present in solution. Moreover, the MAG-bead-based strategy was shown to allow a significantly greater amount of immobilization of surface antibodies because of the large number of particles with a net high surface area.[51] These high-density antibody-carrying beads are expected to facilitate a greater rate of association with surface GAD-65 molecules and slower dissociation when the interactions are strong (Table 1). A prior report estimated that over 100 000 molecules of antibody can be bound selectively to MAG-beads (1 μm) to obtain attomolar detection limits of prostate-specific antigen.[44,51]

Validation of the Graphene-COOH- and MPA-Modified Serum-GADA Immunosensors. DPV was employed as a complementary method to the impedimetric immunosensor. Decreases in DPV-peak currents were observed with increases in serum-GADA−MAG-bead binding to surface GAD-65. This is because the insulating feature imparted on the electrode surface by the MAG−protein A/G−GADA beads bound to GAD-65 is expected to decrease the redox currents of added ferri/ferrocyanide probe in solution (Figure S7). The DPV results correlate with those from EIS. The limits of detection were 34 and 92 pg mL^{-1} for the graphene-COOH- and MPA-modified immunosensors, respectively, which were slightly lower than those from the EIS method. Langmuir-type adsorption kinetics was observed with the DPV responses, which were fit with a linear-regression equation to obtain apparent-equilibrium-dissociation-constant (K_D^{app}) values for both graphene-COOH- and MPA-surface-modified immunoassemblies (Figure S8).

Figure S9 shows the decrease in oscillation frequency monitored in real-time during the covalent immobilization of GAD-65 onto MPA-monolayer- or graphene-COOH-modified QCM gold crystal surfaces. The immobilized amount of GAD-65, calculated by the Sauerbrey equation, was 0.65 ± 0.11 μg cm^{-2} on the MPA surface and 1.41 ± 0.38 μg cm^{-2} on the graphene-COOH surface. This corresponds to a ∼2-fold higher mass density of GAD-65 immobilization on graphene-COOH over that on the MPA surface.

Estimation of the Relative Surface Carboxyl Groups on Graphene-COOH- and MPA-Modified Gold Surfaces. Figure 4A,B shows the cyclic voltammograms of the graphene-COOH- and MPA-coated electrodes covalently attached and electrostatically adsorbed with redox-active aminoferrocene molecules (voltammograms a and b in each plot). The resulting peak currents and integrated peak areas (charges in Coulombs) are directly proportional to the amounts of aminoferrocene molecules bound to either the graphene-COOH or MPA surface. No redox peaks were detected in either the graphene-COOH or MPA surface not immobilized with aminoferrocene, confirming no interferences from the surface modifications on the −COOH estimation (Insets of

DOI: 10.1021/acs.analchem.8b01565
Anal. Chem. 2018, 90, 12456−12463

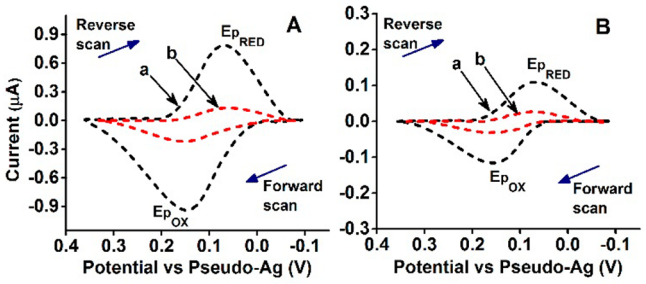

Figure 4. Background-subtracted CVs of (A) graphene-COOH- and (B) MPA-modified gold electrodes with covalently attached (curve a) and adsorbed (curve b) films of aminoferrocene in argon-purged PBS buffer (pH 7.4) at 23 °C. The scan rate was 0.1 V s^{-1}.

Figure S10A,B). The linear dependence of the anodic current with the scan rate suggested that the voltammetry of the aminoferrocene molecules exhibited a surface-confined redox process (Figures S10C,D).

The average formal potentials of the covalently attached aminoferrocene film on the graphene-COOH and MPA surfaces were 112 ± 5 and 114 ± 8 mV, respectively. The electrostatically adsorbed films of aminoferrocene on each of the modified surfaces exhibited similar formal potentials to those of the covalent films. However, the covalent films enabled higher electroactive aminoferrocene immobilization than the electrostatic films, as discussed below.

From the measured oxidation-peak area, the electroactive surface coverage (Γ, eq 1) of aminoferrocene and in turn the relative extent of carboxyl groups were determined.[52] Q is the area of the oxidation peak of aminoferrocene, n is the number of electrons involved in the aminoferrocene oxidation (n = 1), F is the Faraday's constant, and A is the area of the working electrode (A = 0.2 cm^2).

$$\Gamma = Q/nFA \tag{1}$$

The Γ values were also calculated from the anodic peak current by using eq 2,[53] where I_p is the anodic peak current, υ is the scan rate, R is the universal gas constant (8.314 J mol^{-1} K^{-1}), and T (296 K) is the temperature in Kelvin.

$$I_p = n^2F^2\upsilon A\Gamma/4RT \tag{2}$$

The peak-area and peak-current-based estimations of Γ agreed well with each other. The graphene-COOH surface provided a 9-fold greater amount of surface carboxyl groups than the MPA-monolayer surface for the covalent films (Table 2).

The C 1s regions in the XPS spectra of the graphene-COOH and MPA monolayer coated on gold surfaces are presented in Figure S11. The XPS data were analyzed for carbon atoms from different functional groups, such as C−C at 284.8 eV, C−O in the epoxy or ether at ∼286.0 eV, and C═O at ∼288.0 eV.[54,55] As expected, the carboxyl groups from the graphene-COOH-modified gold surface are greater than those from the MPA-modified gold surface, which would thus provide more sites for covalent attachment of the GAD-65 antigen via amide bonds. The XPS finding correlated well with the electroactive quantitation of surface −COOH linked aminoferrocene molecules and the immobilized mass of GAD-65 estimated using QCM.

Application to T1D-Patient Samples and Validation by a Commercial ELISA Kit. We determined that the designed immunosensor platform was applicable for measuring serum GADA concentrations in T1D-patient serum samples. The samples were prepared in a similar manner to those of the GADA-spiked serum standards and captured onto MAG−protein A/G beads for detection upon binding to surface-immobilized GAD-65. A good correlation was obtained between our electrochemical immunoassay and the commercial ELISA kit (paired t test performed at a 95% confidence level). The dynamic range was sufficient to determine the sample GADA concentrations with good precision (Table 3).

Table 2. Estimated Electroactive Amounts of Aminoferrocene on Graphene-COOH- and MPA-Modified Electrodes[a]

parameter	graphene-COOH	MPA
Covalently Attached Aminoferrocene		
Q (nC)	920.3 ± 86.6	98.1 ± 5.9
calculated Γ (pmol cm^{-2})	47.6 ± 5.1	5.1 ± 0.3
I_p (nA)	918.2 ± 76.2	108.3 ± 5.9
calculated Γ (pmol cm^{-2})	48.6 ± 4.2	5.7 ± 0.6
Adsorbed Aminoferrocene		
Q (nC)	189.4 ± 15.4	31.0 ± 1.9
calculated Γ (pmol cm^{-2})	9.8 ± 1.3	1.6 ± 0.11
I_p (nA)	208.2 ± 28.3	34.2 ± 1.3
calculated Γ (pmol cm^{-2})	11.2 ± 2.5	1.8 ± 0.2

[a]The estimations are based on the anodic peak areas (Q, in nC) or peak currents (I_p, in nA) from cyclic voltammograms (eqs 1 and 2).

Table 3. Results from the Analysis of Patient Samples (10% Serum) with the Designed Graphene-COOH Electrochemical Immunosensor and with ELISA (N = 3) and Recovery Data of the Designed EIS Immunoassay and of the ELISA Method for a Patient Serum Sample Spiked with a Known Concentration of GADA

results from patient samples		
T1D-patient samples	EIS immunosensor (ng mL^{-1})	ELISA (ng mL^{-1})
1	3.4 ± 0.2	3.0 ± 0.1
2	2.2 ± 0.3	1.9 ± 0.2

recovery data			
method	spiked [GADA] (ng mL^{-1})	measured [GADA] (ng mL^{-1})	recovery (%)
EIS	0.50	0.45	90
	2.50	2.34	94
ELISA	0.50	0.46	92
	2.50	2.43	97

To assess the accuracy of our electrochemical assay, a known concentration of GADA was spiked into one of the patient serum samples. A recovery percentage of ≥90% was obtained from the electrochemical assay, which was comparable to the recovery using ELISA (Table 3). The electrochemical immunoassay presented took less time than the ELISA method (EIS: immunoassay ∼2.5 h vs ELISA: ∼4 h), requires smaller sample volumes (EIS immunoassay: 3.5 μL per electrode vs ELISA: 100 μL of sample per well), and had a reasonably good linear range (EIS immunoassay: 0.02−2.0 ng mL^{-1} vs ELISA: 0.16−5.0 ng mL^{-1}).

CONCLUSIONS

The presented graphene-modified immunosensor array successfully measured serum GADA levels at clinically relevant

DOI: 10.1021/acs.analchem.8b01565
Anal. Chem. 2018, 90, 12456−12463

concentrations. The selectivity of GAD-65 on the sensor surface was useful for capturing GADA carried by MAG−protein A/G beads in the presence of other unrelated serum antibodies. The use of protein A/G coated MAG beads to separate GADA from serum samples minimized the effects of interferences from the serum matrix and thus enhanced the detection sensitivity. Electrochemical and surface-plasmon methods correlated with each other. Plasmon-enhancing graphene-COOH offered better analytical detection features compared with a self-assembled monolayer of MPA. A good, statistically valid correlation was obtained for the electrochemical immunosensor with the commercial ELISA. Overall, the binding-constant parameter can be used as an excellent quality-control checkpoint for the large-scale production of graphenyl biosensors for reliable applications in clinical diagnostic assays.

■ ASSOCIATED CONTENT

Supporting Information

The Supporting Information is available free of charge on the ACS Publications website at DOI: 10.1021/acs.analchem.8b01565.

Detailed experimental section; SEM, FTIR, Raman, and XPS characterizations of the sensor surface; quantitative data for carboxyl groups and GAD-65 on the sensor surface; and kinetic analysis of antigen−antibody binding (PDF)

■ AUTHOR INFORMATION

Corresponding Author

*E-mail: gopan.krishnan@okstate.edu.

ORCID

Steven L. Suib: 0000-0003-3073-311X

A. Kaan Kalkan: 0000-0001-5878-3413

Sadagopan Krishnan: 0000-0002-9968-2712

Present Address

¶M.K.P.: School of Studies in Life Sciences, Pandit Ravishankar Shukla University, Raipur 492010, Chhattisgarh, India

Author Contributions

⊥G.P. and J.N. contributed equally.

Notes

The authors declare no competing financial interest.

■ ACKNOWLEDGMENTS

We thank Oklahoma State University for financial support. A.K.K. acknowledges the National Science Foundation, Award #1707008. We extend our thanks to Ms. Zainab Al Mubarak for help with the graphical abstract preparation.

■ REFERENCES

(1) Wasserfall, C. H.; Atkinson, M. A. *Autoimmun. Rev.* **2006**, *5*, 424−428.

(2) Morran, M. P.; Vonberg, A.; Khadra, A.; Pietropaolo, M. *Mol. Aspects Med.* **2015**, *42*, 42−60.

(3) Pihoker, C.; Gilliam, L. K.; Hampe, C. S.; Lernmark, Å. *Diabetes* **2005**, *54*, S52−S61.

(4) Atkinson, M. A.; Eisenbarth, G. S. *Lancet* **2001**, *358*, 221−229.

(5) Akerblom, H. K.; Vaarala, O.; Hyöty, H.; Ilonen, J.; Knip, M. *Am. J. Med. Genet.* **2002**, *115*, 18−29.

(6) Ziegler, A.-G.; Nepom, G. T. *Immunity* **2010**, *32*, 468−478.

(7) Gan, M. J.; Albanese-O'Neill, A.; Haller, M. J. *Curr. Probl. Pediatr. Adolesc. Health Care.* **2012**, *42*, 269−291.

(8) Lehuen, A.; Diana, J.; Zaccone, P.; Cooke, A. *Nat. Rev. Immunol.* **2010**, *10*, 501−513.

(9) Pociot, F.; Lernmark, Å. *Lancet* **2016**, *387*, 2331−2339.

(10) Urban, G. J. G.; Friedman, M.; Ren, P.; Törn, C.; Fex, M.; Hampe, C. S.; Lernmark, Å.; Landegren, U.; Kamali-Moghaddam, M. *Sci. Rep.* **2015**, *5*, 11196.

(11) Heding, L. G. *Diabetologia* **1975**, *11*, 541−548.

(12) Andersen, L.; Dinesen, B.; Jorgensen, P. N.; Poulsen, F.; Roder, M. E. *Clin. Chem.* **1993**, *39*, 578−582.

(13) Forest, J. C.; Masse, J.; Lane, A. *Clin. Biochem.* **1998**, *31*, 81−88.

(14) Miao, D.; Guyer, K. M.; Dong, F.; Jiang, L.; Steck, A. K.; Rewers, M.; Eisenbarth, G. S.; Yu, L. *Diabetes* **2013**, *62*, 4174−4178.

(15) Bonaccorso, F.; Sun, Z.; Hasan, T.; Ferrari, A. *Nat. Photonics* **2010**, *4*, 611−622.

(16) Chiu, N.-F.; Huang, T.-Y.; Lai, H.-C.; Liu, K.-C. *Nanoscale Res. Lett.* **2014**, *9*, 445.

(17) Lee, H.; Choi, T. K.; Lee, Y. B.; Cho, H. R.; Ghaffari, R.; Wang, L.; Choi, H. J.; Chung, T. D.; Lu, N.; Hyeon, T.; Choi, S. H.; Kim, D.-H. *Nat. Nanotechnol.* **2016**, *11*, 566−572.

(18) Patil, A. V.; Fernandes, F. B.; Bueno, P. R.; Davis, J. J. *Bioanalysis* **2015**, *7*, 725−742.

(19) Yang, W.; Ratinac, K. R.; Ringer, S. P.; Thordarson, P.; Gooding, J. J.; Braet, F. *Angew. Chem., Int. Ed.* **2010**, *49*, 2114−2138.

(20) Ma, H.; Wu, D.; Cui, Z.; Li, Y.; Zhang, Y.; Du, B.; Wei, Q. *Anal. Lett.* **2013**, *46*, 1−17.

(21) Shanbhag, V. K. L.; Prasad, K. S. *Anal. Methods* **2016**, *8*, 6255−6259.

(22) Pu, Y.; Zhu, Z.; Han, D.; Liu, H.; Liu, J.; Liao, J.; Zhang, K.; Tan, W. *Analyst* **2011**, *136*, 4138−4140.

(23) Yagati, A. K.; Park, J.; Cho, S. *Sensors* **2016**, *16*, 109.

(24) Son, S. J.; Reichel, J.; He, B.; Schuchman, M.; Lee, S. B. *J. Am. Chem. Soc.* **2005**, *127*, 7316−7317.

(25) Connolly, D.; Currivan, S.; Paull, B. *Proteomics* **2012**, *12*, 2904−2917.

(26) Zeng, S.; Baillargeat, D.; Ho, H. P.; Yong, K. T. *Chem. Soc. Rev.* **2014**, *43*, 3426−3452.

(27) Singh, V.; Krishnan, S. *Anal. Chem.* **2015**, *87*, 2648−2654.

(28) Ríos, A.; Zougagh, M.; Bouri, M. *Anal. Methods* **2013**, *5*, 4558−4573.

(29) Bao, F.; Yao, J. L.; Gu, R. A. *Langmuir* **2009**, *25*, 10782−10787.

(30) Nam, J. M.; Thaxton, C. S.; Mirkin, C. A. *Science* **2003**, *301*, 1884−1886.

(31) Thaxton, C. S.; Elghanian, R.; Thomas, A. D.; Stoeva, S. I.; Lee, J. S.; Smith, N. D.; Schaeffer, A. J.; Klocker, H.; Horninger, W.; Bartsch, G.; Mirkin, C. A. *Proc. Natl. Acad. Sci. U. S. A.* **2009**, *106*, 18437−18442.

(32) Zhao, X.; Shippy, S. A. *Anal. Chem.* **2004**, *76*, 1871−1876.

(33) Singh, V.; Nerimetla, R.; Yang, M.; Krishnan, S. *ACS Sens.* **2017**, *2*, 909−915.

(34) Mani, V.; Chikkaveeraiah, B. V.; Rusling, J. F. *Expert Opin. Med. Diagn.* **2011**, *5*, 381−391.

(35) Paleček, E.; Fojta, M. *Talanta* **2007**, *74*, 276−290.

(36) Adam, V.; Huska, D.; Hubalek, J.; Kizek, R. *Microfluid. Nanofluid.* **2010**, *8*, 329−339.

(37) Laschi, S.; Centi, S.; Mascini, M. *Bioanal. Rev.* **2011**, *3*, 11−25.

(38) Kamin, R. A.; Wilson, G. S. *Anal. Chem.* **1980**, *52*, 1198−1205.

(39) Premaratne, G.; Nerimetla, R.; Matlock, R.; Sunday, L.; Hikkaduwa Koralege, R. S.; Ramsey, J. D.; Krishnan, S. *Catal. Sci. Technol.* **2016**, *6*, 2361−2369.

(40) Niroula, J.; Premaratne, G.; Ali Shojaee, S.; Lucca, D. A.; Krishnan, S. *Chem. Commun.* **2016**, *52*, 13039−13042.

(41) Walikonis, J. E.; Lennon, V. A. *Mayo Clin. Proc.* **1998**, *73*, 1161−1166.

(42) Lee, K. B.; Park, S.; Mirkin, C. A. *Angew. Chem.* **2004**, *116*, 3110−3112.

DOI: 10.1021/acs.analchem.8b01565
Anal. Chem. 2018, 90, 12456−12463

(43) Shen, M.; Joshi, A. A.; Vannam, R.; Dixit, C. K.; Hamilton, R. G.; Kumar, C. V.; Rusling, J. F.; Peczuh, M. W. *ChemBioChem* **2018**, *19*, 199−202.
(44) Krishnan, S.; Mani, V.; Wasalathanthri, D.; Kumar, C. V.; Rusling, J. F. *Angew. Chem., Int. Ed.* **2011**, *50*, 1175−1178.
(45) Stoeva, S. I.; Lee, J. S.; Smith, J. E.; Rosen, S. T.; Mirkin, C. A. *J. Am. Chem. Soc.* **2006**, *128*, 8378−8379.
(46) Santos, E. J.; Kaxiras, E. *Nano Lett.* **2013**, *13*, 898−902.
(47) Grigorenko, A. N.; Polini, M.; Novoselov, K. S. *Nat. Photonics* **2012**, *6*, 749−758.
(48) Schedin, F.; Lidorikis, E.; Lombardo, A.; Kravets, V. G.; Geim, A. K.; Grigorenko, A. N.; Novoselov, K. S.; Ferrari, A. C. *ACS Nano* **2010**, *4*, 5617−5626.
(49) Walgama, C.; Al Mubarak, Z. H.; Zhang, B.; Akinwale, M.; Pathiranage, A.; Deng, J.; Berlin, K. D.; Benbrook, D. M.; Krishnan, S. *Anal. Chem.* **2016**, *88*, 3130−3135.
(50) Nogues, C.; Leh, H.; Langendorf, C. G.; Law, R. H. P.; Buckle, A. M.; Buckle, M. *PLoS One* **2010**, *5*, No. e12152.
(51) Mani, V.; Wasalathanthri, D. P.; Joshi, A. A.; Kumar, C. V.; Rusling, J. F. *Anal. Chem.* **2012**, *84*, 10485−10491.
(52) Booth, M. A.; Kannappan, K.; Hosseini, A.; Partridge, A. *Langmuir* **2015**, *31*, 8033−8041.
(53) Bard, A. J.; Faulkner, L. R. *Electrochemical Methods: Fundamentals and Applications*, 2nd ed.; Wiley: Hoboken, NJ, 2001.
(54) Stankovich, S.; Dikin, D. A.; Piner, R. D.; Kohlhaas, K. A.; Kleinhammes, A.; Jia, Y.; Wu, Y.; Nguyen, S. T.; Ruoff, R. S. *Carbon* **2007**, *45*, 1558−1565.
(55) Park, S.; An, J.; Piner, R. D.; Jung, I.; Yang, D.; Velamakanni, A.; Nguyen, S. T.; Ruoff, R. S. *Chem. Mater.* **2008**, *20*, 6592−6594.

DOI: 10.1021/acs.analchem.8b01565
Anal. Chem. 2018, 90, 12456−12463